applied sciences

MDPI

Article

Over and beyond the Primate *baubellum* Surface: A "Jewel Bone" Shielded in Museums

Federica Spani [1,2,*], Maria Pia Morigi [3,4], Matteo Bettuzzi [3,4], Massimiliano Scalici [2] and Monica Carosi [2,*]

[1] Diagnostic Imaging Unit, Departmental Faculty of Medicine and Surgery, Campus Bio-Medico University of Rome, Via Álvaro del Portillo 200, 00128 Rome, Italy
[2] Department of Sciences, Roma Tre University, Viale Guglielmo Marconi 446, 00146 Rome, Italy; massimiliano.scalici@uniroma3.it
[3] Department of Physics and Astronomy "Augusto Righi", Bologna University, Viale Berti Pichat 6/2, 40127 Bologna, Italy; mariapia.morigi@unibo.it (M.P.M.); matteo.bettuzzi@unibo.it (M.B.)
[4] National Institute for Nuclear Physics, Bologna Division, Viale Berti Pichat 6/2, 40127 Bologna, Italy
* Correspondence: f.spani@unicampus.it (F.S.); monica.carosi@uniroma3.it (M.C.)

Abstract: Computed Tomography (CT), mostly used in the medical field, has also recently been involved in Cultural Heritage studies, thanks to its efficiency and total non-invasiveness. Due to the large variety of sizes and compositions typical of Cultural Heritage objects, different X-ray sources, detectors, and setups are necessary to meet the different needs of various case studies. Here, we focus on the use of micro-CT to explore the morphology and shape of a small, neglected bone found inside the clitoris of non-human primates (the *baubellum*), which we obtained by accessing two prestigious primatological collections of the American Museum of Natural History (New York, NY, USA) and the National Museum of Natural History (Washington, DC, USA). Overcoming methodological limits imposed by the absence of homologous landmarks, we combined the use of the non-invasive 3D micro-CT and a recently released landmark-free shape analysis (the alpha-shape technique) to objectively describe and quantify the shape complexity of scanned primate *baubella*. Micro-CT provided high-resolution results, overcoming constraints linked to museum policy about non-disruptive sampling and preserving samples for future research. Finally, it proved appropriate as post-mortem sampling had no impact on protected wild primate populations.

Keywords: clitoral bone; micro-CT; alpha-shapes; 3D rendering

Citation: Spani, F.; Morigi, M.P.; Bettuzzi, M.; Scalici, M.; Carosi, M. Over and beyond the Primate *baubellum* Surface: A "Jewel Bone" Shielded in Museums. *Appl. Sci.* **2022**, *12*, 2096. https://doi.org/10.3390/app12042096

Academic Editors: Alice Dal Fovo and Raffaella Fontana

Received: 31 December 2021
Accepted: 15 February 2022
Published: 17 February 2022

1. Introduction

Nowadays, among a variety of diagnostic imaging tools in the medical field, the use of Computed Tomography (CT) has been shown to be the most widely used. Recently, its importance and potential have become increasingly evident even when applied to other areas, such as industry and Cultural Heritage [1]. A growing number of authors have reported the successful use of CT as an efficient and non-destructive tool for the study of, for example, archaeological findings and works of art [2–15].

CT can be considered the natural evolution of radiography, being capable of providing both morphological and physical information on the inner structure of the objects. In fact, in conventional radiography, the 3D structure of an object is projected onto a 2D detector, and each point of the resulting image provides a measure of the overall attenuation of the X-ray beam as it crosses through the subject. Consequently, while the specimen's lateral dimensions (height and width) are retained on the radiograph, the third dimension (depth) is lost. In general, in the case of essentially bi-dimensional works of art, such as paintings, this is not a crucial issue, but it may create problems when a case study is a tri-dimensional object [16]. The 3D reconstruction of the objects makes it possible to obtain a large amount of information not only on the conservation status and inner morphological features (e.g., useful for conservation and restoration purposes) but also

on the manufacturing and construction technique of a specific artifact (e.g., of a work of art). Information can be retrieved as either 2D cross-section images (the so-called slices) or 3D full-volume images, thus allowing for the inspection and classification of the different materials making up the object studied. Thanks to the use of sophisticated computer programs, it is possible to manipulate the 3D renderings, by making virtual cuts on the reconstructed volume or selectively removing some layers to reveal additional information. Moreover, by processing tomographic data, a 3D numerical model of the sample can be obtained for either virtual reality applications, digital archive storage, or the creation of replicas using 3D printing [17,18].

Due to the large variety of sizes and compositions of the target tissues/materials this technique can be applied to, different X-ray sources, detectors, and setups are necessary to meet the different needs of various case studies. The geometrical setup and X-ray beam energy of medical CT scanners, for example, are optimized for the human body, so their application in areas different from the medical field is characterized by strong constraints about the size, shape, and density of the object to be analyzed [16]. This has been the case when medical scanners have been used for the analysis of human mummies [19–26], human and animal bone fossil materials [27,28], and clay/ceramic archaeological artifacts [29–31]. As for size, whereas traditional CT scanners target medium-sized objects (whose minimal voxel size is usually not lower than 0.5 mm—but see [32] for special CT scanners up to 0.2–0.3 mm), large works of art, or else extremely small objects, must rely on specifically enhanced scanners, such as CT systems, which use X-ray sources of up to 200 kV [6], and micro-CT systems, respectively. Micro-CT is a versatile technique that can be successfully applied to different materials, such as small metal objects, jewelry, ceramics [33], prehistoric pottery, stone [34], and organic material, such as wood [35], charcoal [36], textiles, and archaeological food remains [37], insect museum samples [38], fossil and non-fossil teeth [39,40], and bones [41,42].

Non-human animal bones are used by scholars interested in evolutionary history research through the study of bone morphological variation. This kind of study usually requires the collection of a large number of bone samples, and natural history museums all over the world may represent an essential and extraordinary source of specimens. Nevertheless, especially for studying museum samples, it is necessary to apply non-invasive methodologies of investigation that allow both preserving sample integrity and following strict museum rules about manipulation and non-destructive sampling. Spani and colleagues [42] established a highly reliable methodological protocol for obtaining high-resolution images of primate small bones (i.e., genital bones, known as *baculum* in males and *baubellum* in females) by applying micro-CT on museum specimens. The use of micro-CT allowed us to overcome museum policy constraints and to investigate both anatomy and morphology while keeping samples fully preserved for future research. Although the study of genital bones in primates has always suffered a widespread omission of both occurrence and morphology data in both sexes, a notable bias disproportionally favors male data, making the study of *baubella* even more urgent (see [43] for more details). In this study, we apply micro-CT focusing on primate *baubella* to contribute to investigating the morphology and shape variation of this neglected bone.

Bone morphology is made up of size, shape, structure, and patterns. The shape has traditionally been the subject of controversial studies (not limited to bones) because it is hard to reliably quantify it objectively. This is, in fact, the assumption of morphometry for reading shape as a set of all geometric information contained in it, after eliminating any distortion effects, such as position and orientation in space, and scale [44]. Shape quantification, not just description, is fundamental to studying its variation in an evolutionary context and to better understand the diversity of life and phenomena, such as adaptation and speciation [45,46]. Thanks to the progress made in the digitization of samples, a variety of new methodologies have been developed to analyze and quantify biological data from 3D shapes. By quantifying the variation of the shape based on multivariate methods, the study

of the covariation either between forms or between forms and extrinsic factors has been carried out (e.g., [47]).

Over the last decade, geometric morphometric (GMM) techniques have radically changed the analysis of shape and form. The GMM techniques analyze coordinates of homologous reference points (i.e., landmarks) that are identified on every specimen studied. When this is possible, GMM has proved extremely useful in the study of morphology in a variety of structures, such as vertebrate skulls [48,49], brachyuran claws [50] and carapace [51], molluscan shells [52–54], insect wings [55], and tree leaves [56]. On the contrary, however, the application of GMM is hard when landmarks are lacking, such as in anthropological artifacts [57], seeds [58], otoliths [59], ribs [60], diaphysis of long bones [61], and genital bones [62,63]. In this respect, therefore, the study of shape variation of genitals in general, and genital bones in particular, represents a challenge, and GMM techniques have been successfully applied only to specific cases (e.g., comparisons among morphologically very similar either conspecific [64–68] or congeneric individuals [69,70]).

In this stimulating methodological scenario, we aimed to investigate morphology and shape variation of primate *baubella*, taking advantage of the primatological collections of two of the most prestigious natural history museums, the American Museum of Natural History (NY, USA) and the National Museum of Natural History (Washington, DC, USA). In particular, our goals were: (1) collecting and visualizing 3D *baubella* volumes by using the non-invasive micro-CT technique, which allows the preservation of sample integrity, following museum rules on non-destructive sampling, and (2) by overcoming constraints imposed by the use of GMM techniques, objectively describing and quantifying shape by applying for the first time on *baubella* a recently proposed landmark-free method known as *alpha-shapes* [62].

2. Materials and Methods

2.1. Female Genital Bone Sampling

Two types of samples were used to analyze the female genital bone occurrence and morphology: (1) a fresh sample and (2) museum samples.

2.1.1. Fresh Sample

The fresh sample of *baubellum* was supplied by Istituti Zooprofilattici Sperimentali (II. ZZ. SS.) which in Italy are responsible for receiving primate corpses (dead for natural causes or trauma/disease) from zoos and/or research institutes and carrying out necropsy investigations aimed at identifying possible risks of zoonoses. To maximize chances to gather samples for our project, an agreement between the Department of Sciences (Roma Tre University) and the Ministry of Health (as the referent for all Italian II.ZZ.SS.) was signed. Thanks to this agreement, whenever a primate cadaver of either sex was available at an IZS, the Authors (FS, MS, MC) were notified, and the sample was obtained. To standardize the section of the external genitals by the IZS veterinarians, a protocol was provided by the Authors (FS, MC) to the II. ZZ. SS., including a sample preservation method (70% ethanol). Samples would later be stored at the Department of Sciences until dissection and bone extraction.

2.1.2. Museum Samples

Museum samples were selected by exploring some of the widest wet museum collections (70% ethanol) of primates belonging to the American Museum of Natural History (AMNH, New York, NY, USA Vertebrate Collection Database available at http://sci-web-001.amnh.org/db/emuwebamnh/index.php, accessed on 1 March 2018) and National Museum of Natural History (Washington DC, USA, Mammal Collection Database available at https://collections.nmnh.si.edu/search/mammals/, accessed on 2 April 2019). Museum samples were either whole bodies or external genitals only. Neither skins nor skeletons were considered in the present study because the taxidermic preparations they are subjected to usually result in a definitive loss of soft tissue (in the former), and a high probability of

loss of smaller skeletal components (such as genital bones) during the boiling process (in the latter).

2.2. Anatomical Data Collection and 3D Morphological Data Acquisition

As part of a wider study of primate genital bones, a 3-step methodological protocol was applied (palpation, X-rays, micro-CT [42]) to obtain a set of data on bone occurrence, anatomical position, and external and internal morphology. Depending on sample type (fresh/museum) and origin (Italy/USA), slight variations to this protocol have been made for (a) micro-CT scanner models and (b) a few necessary methodological adjustments, as reported in Table 1 (see also Table 2 for the micro-CT scanning settings).

Table 1. The methodological protocol followed for each specimen (both fresh and museum) aimed at obtaining both anatomical and 3D morphological data for the *baubellum*.

Samples	Manual Palpation	X-rays	Bone Extraction	Micro-CT	
				Sample Preparation	Scan
	(1st step [42])	(2nd step in [42])		(3rd step in [42])	(3rd step in [42])
Fresh sample (Italy)	Double palpation along both mediolateral and anteroposterior axes performed by two operators (FS, MC)	2D projectional radiography (X-ray plates) shot with Arcom Simply system for veterinary radiodiagnostics (20 ma—40 kV setting) (available at "Enrico Fermi" veterinary clinic, Rome, IT)	Sample positive to the presence of a genital bone was selected for manual dissection. For bone cleaning (tissues leftovers) and whitening, extracted bones were boiled for 30 min into a solution made of 50% oxidane (H_2O) and 50% sodium hydrogen carbonate ($NHCO_3$)	The fresh sample was immobilized in small pieces of polystyrene and placed on the high-precision rotary table to be scanned. The previous bone extraction guaranteed optimal 3D results (bones scanned directly without any surrounding soft tissues), and the 3D post-processing phase was subsequently simplified (see below)	Tomographic system * assembled at the Department of Physics and Astronomy of Bologna University (Italy). The settings used for micro-CT setup are reported in Table 2
Museum wet samples (USA)	Same (performed only by FS)	X-rays performed directly by using the micro-CT scanner	Extraction not allowed	Each sample was packed into plastic bags and immobilized by using various kinds of supports for avoiding sample movements during scanning time due to alcohol evaporation	PHOENIX V | TOME | X S; PHOENIX V | TOME | X M. Settings used for micro-CT setup are reported in Table 2)

* Same used by Spani et al. [42]. More information is available at the following link: http://www.fisica-astronomia.unibo.it/it/dipartimento/servizi-e-strutture/strutture/laboratori-di-ricerca-1/indagini-con-i-raggi-x/radiografia-digitale-e-tomografia-3d (accessed on 8 October 2020).

Table 2. Micro-CT scanners' settings used for either Italian fresh or USA museum samples (auto = automatically set).

	Settings	
Parameters	**(Italy)**	**(USA)**
Voltage (kV)	60–100	auto
Beam current (μA)	80–200	auto
Al filter (mm)	no/1	no/2
N° projection	900	1500–1800
Total rotation angle	360°	360°
Exposure time (s)	0.7–1	1
Voxel size (μm)	9.16–14	18

The final phases of reconstruction, segmentation, and post-processing were performed by using different software depending on sample type/origin: the proprietary software PARREC for the Italian/fresh sample and the Datos software for USA/museum samples, both followed by rendering with VGStudioMax 3.1 (see details in [42]). The total average

time needed to detect and visualize genital bones differed between fresh and museum samples (4 h 50′ and 1 h 30′, respectively, see Table 3). For USA samples, no dissection was performed since it did not fit with museum destructive sampling requirements (Table 3 for museum samples).

Table 3. Total time (T) required to identify, and 3D visualize bones located in the female external genitalia of non-human primates (both fresh and museum specimens).

		Fresh Samples	Museum Samples
Step		**T (min)**	**T (min)**
Manual Palpation		5	2
X-rays		10	3
Dissection		60	n/a
Micro-CT		215	65–95
a	alignment	60	5
b	scan	75	30–60
c	reconstruction	60	20
d	3D rendering	10	10
T total		290	70–100

2.3. Morphological Analysis and Form Variation

2.3.1. Qualitative Analysis

Overall evaluation of *baubellum* external morphology has been made based on both actual bone appearance (i.e., dissections and extractions, applied only to the fresh sample) and 3D scans. The internal morphology of scanned *baubella* has been investigated only after the scan process, thus allowing the examination of inner parts, preserving sample integrity, and making it available for future studies.

2.3.2. Quantitative Analysis

To study shape variation, it was necessary to overcome the difficulties related to the extreme morphological variability that affects the *baubellum* and that did not allow the identification of homology points and the use of spatial landmarks (i.e., anatomical *loci* recognizable in all samples) necessary to analyze geometric morphometry. Thus, to quantify the 3D morphological complexity and obtain a continuous variable summarizing the 3D surface shape variation of scanned *baubella*, we applied a recently established landmark-free technique known as '*alpha-shapes*' analysis [62,63]. 'Complexity' was measured as the degree of sophistication required for the volume of an appropriately fitted 'alpha' shape to match the 3D model of a *baubellum*. The procedure used is summarized below:

1. The product of segmentation (see 'Anatomical data collection and 3D morphological data acquisition' section) was extracted either as a 3D polygonal volumetric model (file format: ply) or mesh. The polygonal models were post-processed with Amira and Geomagic Studio 2014 software.
2. The total number of polygons was taken down to 250,000 in Amira, and the extracted surface, loaded into Geomagic Studio 2014, was corrected by deleting (automatically and manually) computational errors in the mesh, such as non-manifold edges, self-intersections, highly creased edges, spikes, small components, small tunnels, and small holes. Only the external surface of bones was kept, by emptied 3D models, to avoid anatomical non-homologies in the bone's internal structure. In addition, each *baubellum* length was measured by using the distal and proximal ends of the bones as reference points. The length was recorded 3 times by the same operator (FS), and the mean was calculated.
3. The mesh was converted to a point cloud with Meshlab software, and the total number of points making up the cloud was set to 100,000.
4. An 'alpha-shape' is formed by the boundary of an alpha complex, which, in turn, is a sub-complex of the Delaunay triangulation for a given set of points [71]. For a

given set of points in space, a family of 'alpha-shapes' can be defined, ranging from a conformation that fits the set of points very coarsely (forming a convex 'shell' around the points) to a conformation that fits very finely around the points. The following equation was used to calculate the typical radius α for each individual:

$$\alpha = k \times l_{ref}$$

where α is the radius, k is the refinement coefficient, and l_{ref} is the reference length (for more details see [62,63]).

5. Since the present study is only interested in quantifying shape complexity regardless of size, all α-rays were scaled to the overall mesh size summarized by the l_{ref} factor. The size factor was then calculated as the average of the average distances of each point of the cloud from the 100 closest ones.
6. The complexity of the *baubella* shapes analyzed in 3D was visualized by graphing the trend of a curve (representative of this morphological complexity) given by the ratio of the variables k to the percentage of the CT volume as described by the volume of the alpha-shapes; furthermore, morphological complexity was also quantified by the *1/k* ratio, as suggested by Brassey and collaborators [63].

Steps 4 through 6 were performed in R software, and scripts are available under motivated request to the Author (FS).

3. Results

3.1. 3-Step Protocol and baubellum Occurrence Data

Six samples of female external genitalia (including 3 clitoris and 3 whole bodies, based on the availability of both museum and fresh samples) were analyzed using the methodology proposed by Spani and collaborators ([42]; 3-step protocol) and the results are summarized in Table 4 (including comparison with available scientific literature).

All 3 clitoral samples belonged to adult specimens: (1) *Cebus capucinus* (capuchin monkey, museum collection of the NMNH); (2) *Varecia variegata* (black-and-white ruffed lemur, museum collection of the AMNH); (3) *Lemur catta* (ring-tailed lemur, fresh sample from the I.Z.S. di Lazio e Toscana). The first two specimens proved positive at all steps of the 3-step protocol [42] (Figure 1A,F), while the third one proved negative at the first step (i.e., palpation) and then positive at the last 2 (Figure 1C). Three whole bodies scanned belonged to 3 adult specimens (1) *Galagoides demidoff* (Demidoff's galagon), (2) *Otolemur crassicaudatus* (giant brown galago), and (3) *Propithecus verreauxi* (Verreaux's sifaka; all specimens from the museum collection of the AMNH). All these samples tested positive for *baubellum* presence at all steps of the 3-step protocol (Figure 1B,D,E).

Table 4. List of samples (alphabetic order for genera) of female external genitals analyzed for this study (N = 6 specimens representing 6 genera and 6 species). Information provided for each specimen: source (AMNH—American Museum of Natural History, USA; NMNH—National Museum of Natural History, USA; IZSLT—Istituto Zooprofilattico Sperimentale Lazio e Toscana); identification number (ID); updated taxonomy; age class; specimen type (whole body or clitoris); data available in the literature (Lit.; DD = Data deficient, data not available in the literature; 1 = *baubellum* presence; 0 = *baubellum* absence); data of the present study obtained by applying the methodological 3-step protocol shown in Table 1 (Palp. = palpation; X-Ray = radiography; micro-CT = micro-computed tomography).

						Present Study Data		
Source	**ID**	**Taxonomy**	**Age-Class**	**Specimen**	**Lit.**	**Palp. (1st Step)**	**X-ray (2nd Step)**	**Micro-CT (3rd Step)**
NMNH	257679	*Cebus capucinus*	Adult	Clitoris	1	1	1	1
AMNH	50984	*Galago demidoff*	Adult	Whole-body	1	1	1	1
IZSLT	22899	*Lemur catta*	Adult	Clitoris	1	0	1	1
AMNH	202613	*Otolemur crassicaudatus*	Adult	Whole-body	1	1	1	1
AMNH	31256	*Propithecus verreauxi*	Adult	Whole-body	DD	1	1	1
AMNH	170786	*Varecia variegata*	Adult	Clitoris	1	1	1	1

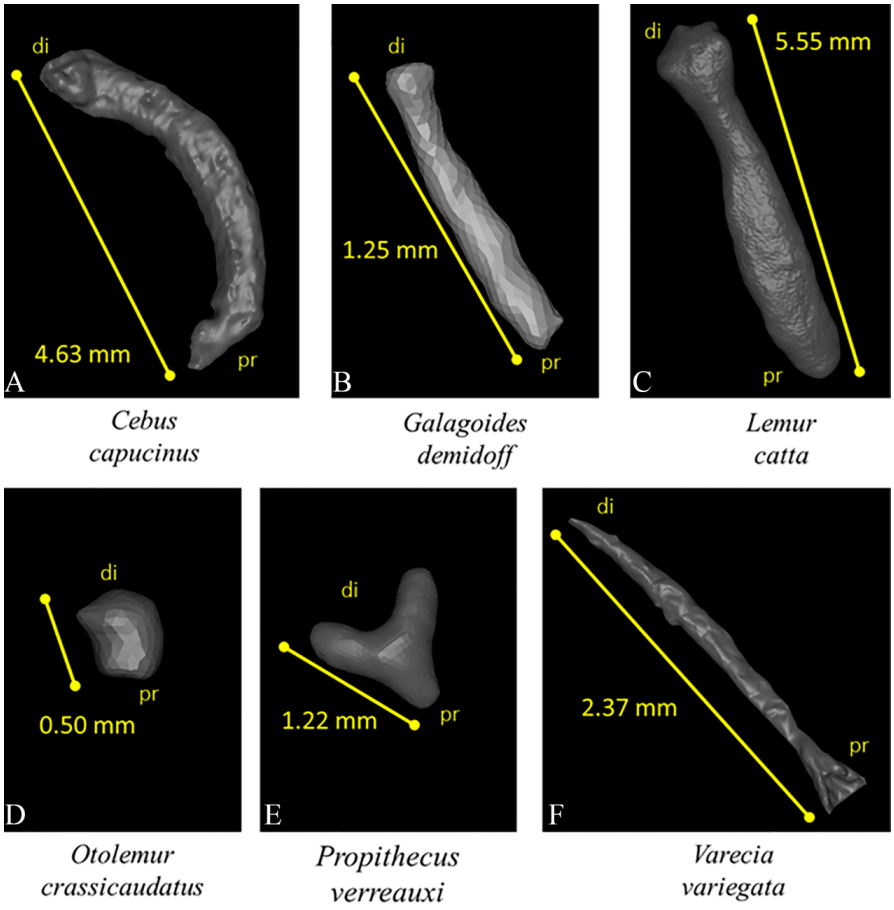

Figure 1. 3D visualization of 6 *baubella* belonging to 6 different primate species with respective proximal-distal lengths (di—distal; pr—proximal). Images not to scale. (**A**) *Cebus capucinus*, (**B**) *Galagoides demidoff*, (**C**) *Lemur catta*, (**D**) *Otolemur crassicaudatus*, (**E**) *Propithecus verreauxi*, (**F**) *Varecia variegata*.

3.2. Anatomical and 3D Morphological Data

Two-dimensional data revealed that all *baubella* are located at the distal end of the clitoris, and bone length (measured from distal to proximal end) ranged from 0.5 mm in *O. crassicaudatus* to 5.55 mm in *L. catta* (Figure 1). Three different morphologies appear: (1) the stick shape (the most common), straight in *G. demidoff*, *V. variegata*, and *L. catta* (Figure 1B,C,F), and curved in *C. capucinus* (Figure 1A); (2) the Y-shape in *P. verreauxi* (Figure 1E); (3) the extremely small and rounded *baubellum* in *O. crassicaudatus* (Figure 1D). Internally, the bony tissue appeared compact overall, and numerous canals (likely Haversian channels) ran through it (see some examples of *baubellum* internal morphology in Figure 2).

3.3. Analysis of α-Shapes

The *alpha-shape* methodology shows and summarizes the complexity of the 3D shape of the scanned *baubella* in a single curve representative of each sample (Figure 3). As the value of the refinement coefficient (k) (in abscissa) decreases, the percentage of the alpha-shape volume that intersects the CT volume also decreases. Below 100%, the alpha-shape "decomposes" and traverses the point cloud. The "optimal" refinement (indicated in Figure 3 as optima) corresponds to the value of the parameter 1/k that describes a continuous variable of the morphological complexity; the optimal value of k is reached when the volume of the alpha-shapes is exactly equal (100%) to the CT volume. On the contrary, excessively high k values correspond to highly coarse alpha-shapes that wrapped the cloud of points adapting only to the outermost points of the cloud itself. Figure 4

shows all the curves obtained as described by a single parameter, the refinement coefficient (k), which facilitates further and subsequent comparative analyses and represents the morphological complexity of the scanned *baubella*.

Figure 2. 3D visualization of *baubella* belonging to 3 species of non-human primates with relative 2D views of the 3 orthogonal sections: axial, sagittal, and frontal. (**A**): *C. capucinus*; (**B**): *L. catta*; (**C**): *V. variegata*.

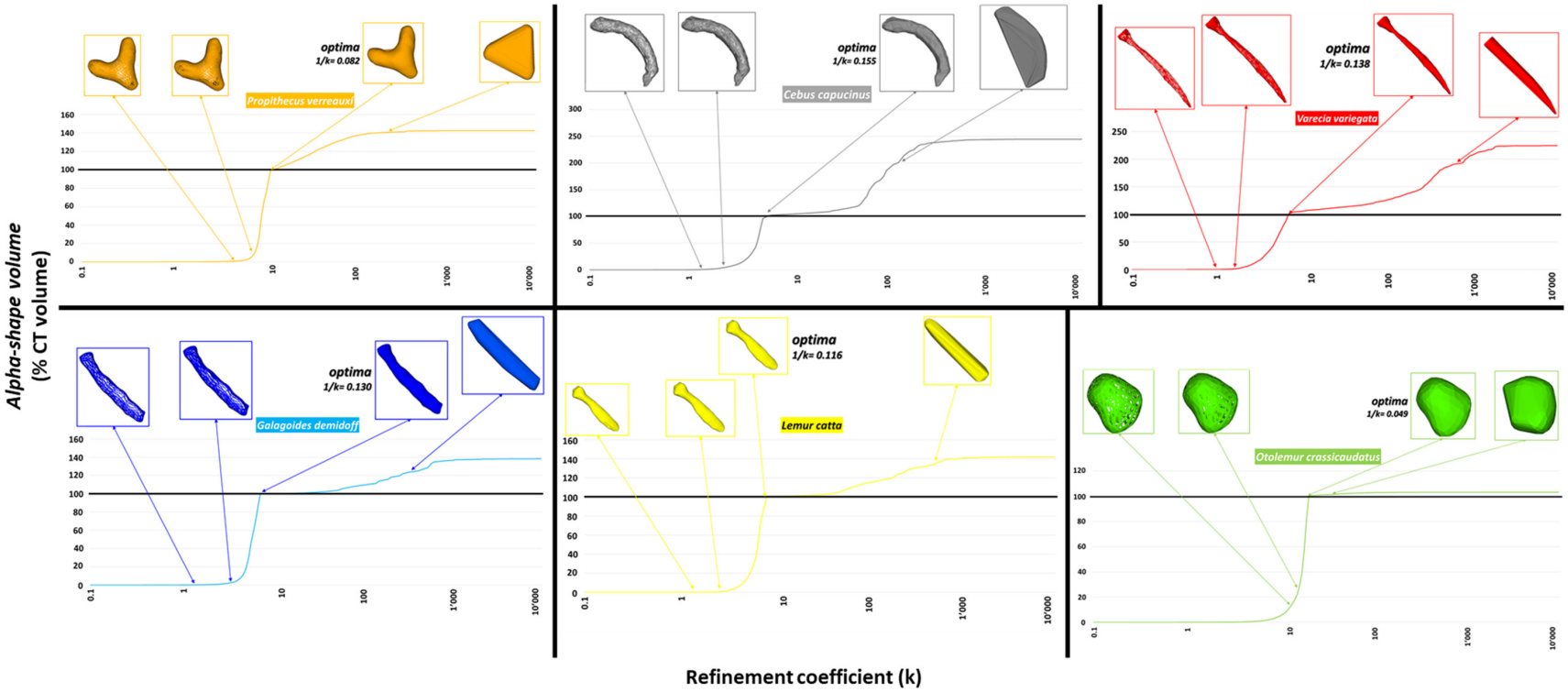

Figure 3. Alpha-shapes were calculated for each of the scanned *baubella*. For each sample, 4 different conformations of the alpha-shapes corresponding to different values of the refinement coefficient (k, in abscissa of all graphs) are shown. From left: the first and second conformation corresponds to values of k such that the volume of the alpha-shapes does not optimally intersect the CT volume; the third conformation is the one corresponding to an optimal value of k (*optima*) such that the volume of the alpha-shapes perfectly intersects the CT volume (intersection of the curves with the black line corresponding to the value of 100%), and the value 1/k is shown as a descriptor of morphological complexity; finally, the fourth conformation is that corresponding to values of k excessively high, such that the volume of the alpha-shapes exceeds the volume CT and appears with a shapeless envelope that wraps the outermost points of the cloud.

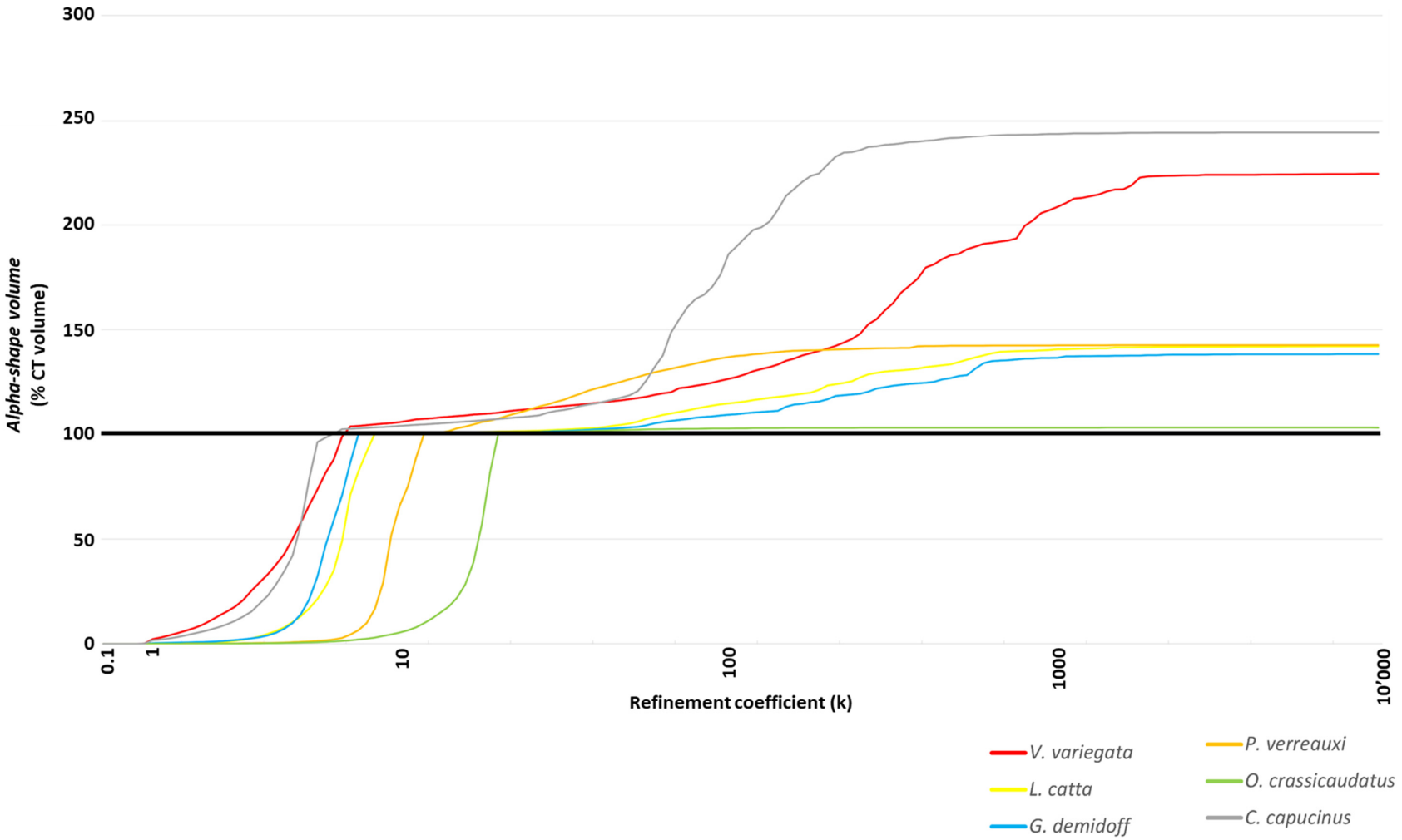

Figure 4. Profiles of alpha-shapes displayed in a single graph: close curves with similar trends describe similar morphological complexities.

4. Discussion

In compliance with the museum's non-destructive sampling rules, anatomical and 3D morphological data were obtained thanks to the application of non-invasive micro-CT. The micro-CT followed by the alpha-shapes analysis proved appropriate to describe a variety of traits (i.e., shape, surface, length, internal structure) in the museum (and fresh) *baubellum* specimens, both at the specific and the comparative inter-specific level, disentangling morphological differences among species. All samples of the clitoris revealed a *baubellum* inside regardless of specimen type (i.e., either museum/fresh or clitoris/whole body). For almost all species (*C. capucinus*, *G. demidoff*, *L. catta*, *O. crassicaudatus*, and *V. variegata*), our occurrence data confirmed the literature data ([72–76] respectively). More importantly, for *P. verreauxi* no information is available in the literature so far; thus, our datum of *baubellum* presence represents the first report for the species.

Overall, forms reconstructed and visualized in 3D appeared rather variable both in size (length ranging from less than a millimeter to little more than 5 mm) and shape. Three different shape types were unfolded that we defined as 'stick' (more or less curved), 'Y', and rounded type. According to the only one scanned sample of primate *baubellum* previously described [42], the surface of our *baubellum* samples appeared smooth and coherent (also compared with the rough and jagged surface described for the *baculum* of *Mandrillus sphinx* [42]. In all samples, the internal morphology showed a very similar internal arrangement, including the Haversian channels, as already observed in *Sapajus apella baubellum* (Linnaeus, 1758) [42].

Alpha shape profiles of scanned 3D surfaces allowed us to characterize and finally quantify *baubellum* shapes. Specifically, similar/dissimilar external morphologies were marked out by comparing (a) the trend of the curves (qualitative evaluation) and (b) the optimal refinement coefficient "1/k" (quantitative evaluation). As shown in Figure 4, all *baubella* recognized as a morphological type similar to a 'stick' (i.e., *C. capucinus*, gray line; *G. demidoff*, blue line; *L. catta*, yellow line; *V. variegate*, red line) are described by profiles with a similar trend. Accordingly, the values of k at which the volumes of the alpha-shapes reach 100% of the CT volumes were close, as the corresponding values of the 1/k parameters showed in Figure 3 (*C. capucinus* = 0.15; *G. demidoff* = 0.13, *L. catta* = 0.11; *V. variegata* = 0.13). On the contrary, alpha shape profiles of the other two morphological types showed different trends (both between them and also in comparison with the 'stick' types), as shown by the green line of the rounded *baubellum* type (i.e., *O. crassicaudatus*) and the orange line of the 'Y' type (i.e., *P. verreauxi*). As expected, 1/k parameters resulted far from each other (1/k = 0.049 and 1/k = 0.082, respectively) and from those of the 'stick' type. It is, therefore, appropriate to affirm that for *baubella* that are externally very similar (or dissimilar) to each other, the relationship between the percentage of CT volume (described by the volume of the alpha-shapes) and the refinement coefficient (k) is characterized by very similar (or dissimilar) profiles, with close (or far) values of the parameter 1/k.

We aimed to obtain quantitative data about shape description and variation on a challenging bone by accessing precious museum reserves and by applying a combination of non-invasive data acquiring techniques and landmark-free techniques. Although overall research on genital bones is still far from being exhausted, no quantitative study about their morphological evolution, however, has ever tried to investigate the evolution of shape in such diverse bones, but has rather focused on size only, even represented by a very simple estimate such as length [77–81]. One crucial reason that explains the focus on length rather than on shape may lie in the difficulties of finding, on bone surface, the homologous references (landmarks) at the interspecific level, which are essential to apply the appropriate geometric morphometrics. The development of automated landmark-free methods has recently been stimulated by the necessity of quantifying shape in all those biological structures that are deficient in homologous points, and the *alpha-shapes* method [62] proved extremely useful for our specific aim. An alternative landmark-free method proposed by Pomidor and colleagues [82] is the Generalized Procrustes Surface Analysis (GPSA). However, the GPSA technique could not be applied to the present study

due to the impossibility of controlling the superimposition process (i.e., the centering, rotating, and scaling of all surfaces at the same point in the space, in the same orientation, and at the same dimension, respectively [72,83,84]). Specifically, if applied to our scans, the distal end of a *baubellum* could theoretically be erroneously aligned in the space onto the proximal end of another bone due to dummy homologies. The alpha shape methodology allowed us to overcome the problem of uncontrolled alignment by comparing several surfaces independently.

In addition, our focus centered on the shape quantification of the most neglected primate genital bone, the *baubellum*. Based on the bias found in the literature about variation in genital morphology, which returns data and discussions mostly limited to the male's genital external and internal features (e.g., penile length and complexity of distal morphology, the size, and shape of keratinized spines, *baculum* occurrence, length, and width, descriptive morphology [85,86]), we considered it mandatory (and fair) to enhance and initiate implementing the literature status of the *baubellum* (as for occurrence, external and internal morphology, length, and shape quantification data). The paucity of studies on the *baubellum* (as well as the clitoris) is even more striking by considering that: (a) it is not limited to the primate order but it also applies to upper taxonomic levels (i.e., mammals) and (b) although *baculum* (and penis) and *baubellum* (and clitoris) are homologous structures (i.e., they share ontogeny), most scientific efforts have been always and unjustifiably focused on just the male counterpart ([73,86–91], but see the most recent [43,92,93]).

Most of the world's population of primate species are threatened by extinction [94], therefore the invasive level of analysis usually required for anatomical studies [95] is inappropriate and unacceptable, especially for the primate order. Therefore, data acquisition from museum collection specimens represents a kind of post-mortem sampling that prevents the depletion of protected wild primate populations. In addition, museum collections are even more valorized when non-disruptive 3D scanning is applied since it allows both to produce advanced data from historic material (either exhibited or hidden in basements) and also to protect the integrity of samples thus available for future research to come [42,43]. The *baubellum* still represents a wide and worthy topic to investigate. We believe that a systematic study building up a dataset on quantitative data about shape description and variation would contribute with a refreshingly novel perspective to shed light on the evolutionary history of *baubella* in primates. We hope this study will encourage and open up new opportunities for research about primate *baubellum* phylogenetic distribution (i.e., by filling occurrence gaps), evolutionary developmental biology (i.e., by studying shared ancestry and ontogeny), and adaptive meaning (i.e., by hypothesizing and investigating "mysterious" function(s)), especially taking into account the huge and unexploited materials still available in museums all over the world.

In conclusion, we have been able to overcome methodological limits imposed by the absence of homologous landmarks on *baubella*, and we objectively described and quantified shape complexity by combining the use of the non-invasive 3D micro-CT and the alpha-shape technique. Micro-CT provided high-resolution results, overcoming constraints linked to museum policy about non-disruptive sampling and preserving samples for future research, and it proved appropriate as post-mortem sampling has no impact on protected wild primate populations. By quantifying *baubellum* morphological complexity and variability, we aimed to take the study of the anatomy and morphology of *baubellum* to a higher level to fill knowledge gaps in its evolutionary development, phylogeny, and function(s).

Author Contributions: Conceptualization, M.C.; Methodology, F.S., M.P.M. and M.B.; Software, F.S., M.P.M. and M.B.; Validation, F.S.; Formal Analysis, F.S.; Investigation, F.S.; Resources, F.S., M.S. and M.C.; Data Curation, F.S., M.P.M. and M.B.; Writing—Original Draft Preparation, F.S., M.S. and M.C.; Writing—Review & Editing, F.S., M.S. and M.C.; Visualization, F.S.; Supervision, M.S. and M.C.; Project Administration, M.S. and M.C.; Funding Acquisition, F.S., M.S. and M.C. All authors have read and agreed to the published version of the manuscript.

Funding: This work was supported by: (1) Roma Tre University doctoral funds granted to FS; (2) Grant of Excellence Departments, MIUR-Italy (ARTICOLO 1, COMMI 314–337 LEGGE 232/2016).

Institutional Review Board Statement: Not applicable.

Informed Consent statement: Not applicable.

Data Availability Statement: Data available on request.

Acknowledgments: We are in debt to Claudia Eleni, a veterinarian at Istituto Zooprofilattico Sperimentale di Lazio e Toscana (IZSLT), for providing a fresh sample from a corpse on which necropsy was performed; Francesca Mazzeo, health director of Veterinary Clinic "Enrico Fermi", for allowing use to use her radiography (X-ray) machine; Lu Yao for providing assistance and expertise during museum sampling activities at the American Museum of Natural History (New York, NY, USA).

Conflicts of Interest: The authors declare no conflict of interest.

References

1. Withers, P.J.; Bouman, C.; Carmignato, S.; Cnudde, V.; Grimaldi, D.; Hagen, C.K.; Maire, E.; Manley, M.; Du Plessis, A.; Stock, S.R. X-Ray Computed Tomography. *Nat. Rev. Methods Primers* **2021**, *1*, 18. [CrossRef]
2. Mazansky, C. CT in the study of antiquities: Analysis of a basket-hilted sword relic from a 400-year-old shipwreck. *Radiology* **1993**, *186*, 55A–61A. [PubMed]
3. Rossi, M.; Casali, F.; Chirco, P.; Morigi, M.P.; Nava, E.; Querzola, E.; Zanarini, M. X-ray 3D computed tomography of bronze archeological samples. *IEEE Trans. Nucl. Sci.* **1999**, *46*, 897–903. [CrossRef]
4. Rossi, M.; Casali, F.; Bettuzzi, M.; Morigi, M.P.; Romani, D.; Golovkin, S.V.; Govorun, V.N. Experimental micro-CT system for X-ray NDT. *Proc. SPIE* **2001**, *4503*, 338–348.
5. Applbaum, N.; Applbaum, Y.H. The use of medical computed tomography (CT) imaging in the study of ceramic and clay archaeological artifacts from the ancient near east. In *X-rays for Archaeology*; Uda, M., Demortier, G., Nakai, I., Eds.; Springer: Dordrecht, The Netherlands, 2005; pp. 231–245.
6. Casali, F. X-ray and neutron digital radiography and computed tomography for cultural heritage. In *Physical Techniques in the Study of Art, Archaeology and Cultural Heritage*; Bradley, D., Creagh, D., Eds.; Elsevier: Amsterdam, The Netherlands, 2006; Volume 1, pp. 41–123.
7. Freeth, T.; Bitsakis, Y.; Moussas, X.; Seiradakis, J.H.; Tselikas, A.; Mangou, H.; Zafeiropoulou, M.; Hadland, R.; Bate, D.; Ramsey, A. Decoding the ancient Greek astronomical calculator known as the Antikythera Mechanism. *Nature* **2006**, *444*, 587–591. [CrossRef]
8. Morigi, M.P.; Casali, F.; Bettuzzi, M.; Brancaccio, R.; d'Errico, V. Application of X-ray computed tomography to cultural heritage diagnostics. *Appl. Phys. A* **2010**, *100*, 653–661. [CrossRef]
9. Hughes, S. CT scanning in archeology. In *Computed Tomography—Special Application*; Saba, L., Ed.; InTech: Rijeka, Croatia, 2011; pp. 57–70.
10. Re, A.; Albertin, F.; Bortolin, C.; Brancaccio, R.; Buscaglia, P.; Corsi, J.; Cotto, G.; Dughera, G.; Durisi, E.; Ferrarese, W. Results of the Italian neu_ART project. *IOP Conf. Ser. Mater. Sci. Eng.* **2012**, *37*, 012007. [CrossRef]
11. Re, A.; Corsi, J.; Demmelbauer, M.; Martini, M.; Mila, G.; Ricci, C. X-ray tomography of a soil block: A useful tool for the restoration of archaeological finds. *Herit. Sci.* **2015**, *3*, 1–7. [CrossRef]
12. Pintus, R.; Pal, K.; Yang, Y.; Weyrich, T.; Gobbetti, E.; Rushmeier, H. A survey of geometric analysis in cultural heritage. *CGF* **2016**, *35*, 4–31. [CrossRef]
13. Johnston, R.; Thomas, R.; Jones, R.; Graves-Brown, C.; Goodridge, W.; North, L. Evidence of diet, deification, and death within ancient Egyptian mummified animals. *Sci. Rep.* **2020**, *10*, 14113. [CrossRef]
14. Albertin, F.; Bettuzzi, M.; Brancaccio, R.; Toth, M.B.; Baldan, M.; Morigi, M.P.; Casali, F. Inside the Construction Techniques of the Master Globe-Maker Vincenzo Coronelli. *Microchem. J.* **2020**, *158*, 105203. [CrossRef]
15. Albertin, F.; Baumer, L.E.; Bettuzzi, M.; Brancaccio, R.; Caruso, E.; Casali, F.; Cifarelli, L.; Festa, G.; Griffo, M.G.; Mistretta, A.; et al. X-Ray Computed Tomography to Study Archaeological Clay and Wood Artefacts at Lilybaeum. *Eur. Phys. J. Plus* **2021**, *136*, 513. [CrossRef]
16. Morigi, M.P.; Casali, F. Radiography and Computed Tomography for Works of Art. In *Handbook of X-ray Imaging, Physics and Technology*; Russo, P., Ed.; CRC Press: Boca Raton, FL, USA, 2017; pp. 1185–1210.
17. Laycock, S.D.; Bell, G.D.; Mortimore, D.B.; Greco, M.K.; Corps, N.; Finkle, I. Combining x-ray micro-CT technology and 3D printing for the digital preservation and study of a 19th Century Cantonese chess piece with intricate internal structure. *J. Comput. Cult. Herit.* **2012**, *5*, 1–7. [CrossRef]
18. Doney, E.; Krumdick, L.A.; Diener, J.M.; Wathen, C.A.; Chapman, S.E.; Stamile, B.; Scott, J.E.; Ravosa, M.J.; Van Avermaete, T.; Leevy, W.M. 3D printing of preclinical X-ray computed tomographic data sets. *JoVE* **2013**, *73*, 50250. [CrossRef] [PubMed]
19. Dawson, W.R.; Gray, P.H.K. *Catalogue of Egyptian Antiquities in the British Museum 1: Mummies and Human Remains*; The British Museum Press: London, UK, 1968.
20. Marx, M.; D'Auria, S.H. CT examination of eleven Egyptian mummies. *RadioGraph* **1986**, *6*, 321–330. [CrossRef]

21. Baldock, C.; Hughes, S.W.; Whittaker, D.K.; Taylor, J.; Davis, R.; Spencer, A.J.; Tonge, K.; Sofat, A. 3-D reconstruction of an ancient Egyptian mummy using X-ray computer tomography. *J. R. Soc. Med.* **1994**, *87*, 806–808.
22. Hughes, S. Three-dimensional reconstruction of an ancient Egyptian mummy. In *Imaging the Past*; Higgins, T., Main, P., Lang, J., Eds.; British Museum Press: London, UK, 1996; Volume 114, pp. 211–225.
23. Previgliano, C.H.; Ceruti, C.; Reinhard, J.; Araoz, F.A.; Diez, J.G. Radiologic evaluation of the Llullaillaco mummies. *Am. J. Roentgenol.* **2003**, *181*, 1473–1479. [CrossRef]
24. Taylor, J. *Mummy: The Inside Story*; The British Museum Press: London, UK, 2004.
25. Davis, R. Radiography: Archaeo-human and animal remains. Part I: Clinical radiography and archaeo-human remains. In *Radiography of Cultural Material*; Lang, J., Middleton, A., Eds.; Elsevier: Amsterdam, The Netherlands; Butterworth-Heinemann: Oxford, UK, 2005; pp. 130–149.
26. Lynnerup, N. Medical imaging of mummies and bog bodies—A mini-review. *Gerontology* **2010**, *56*, 441–448. [CrossRef]
27. Lynnerup, N.; Hjalgrim, H.; Nielsen, L.R.; Gregersen, H.; Thuesen, I. Non-invasive Archaeology of Skeletal Material by CT Scanning and Three-dimensional Reconstruction. *Int. J. Osteoarch.* **1997**, *7*, 91–94. [CrossRef]
28. Wu, X.; Schepartz, L.A. Application of computed tomography in paleoanthropological research. *Prog. Nat. Sci.* **2009**, *19*, 913–921. [CrossRef]
29. Anderson, T.; Fell, C. Analysis of Roman cremation vessels by computerized tomography. *J. Arch. Sci.* **1995**, *22*, 609–617. [CrossRef]
30. Minozzi, S.; Giuffra, V.; Bagnoli, J.; Paribeni, E.; Giustini, D.; Caramella, D.; Fornaciari, G. An investigation of Etruscan cremations by Computed Tomography (CT). *Antiquity* **2010**, *84*, 195–201. [CrossRef]
31. Harvig, L.; Lynnerup, N.; Ebsen, J.A. Computed tomography and computed radiography of late Bronze Age cremation urns from Denmark: An interdisciplinary attempt to develop methods applied in bioarchaeological cremation research. *Archaeometry* **2012**, *54*, 369–387. [CrossRef]
32. Logan, H.; Wolfaardt, J.; Boulanger, P.; Hodgetts, B.; Seikaly, H. Evaluation of the accuracy of cone beam computerized tomography (CBCT): Medical imaging technology in head and neck reconstruction. *J. Otolaryngol.—Head Neck Surg.* **2013**, *42*, 1–8. [CrossRef] [PubMed]
33. Sanger, M.; Thostenson, J.; Hill, M.; Cain, H. Fibrous twists and turns: Early ceramic technology revealed through computed tomography. *Appl. Phys. A* **2013**, *111*, 829839. [CrossRef]
34. Yang, M.; Yang, Y.; Wang, C. A new 3D information acquisition method of micro-drilling marks on ancient perforated stone bead through micro-CT. *J. X-ray Sci. Technol.* **2011**, *19*, 333–343. [CrossRef]
35. Haneca, K.; Deforce, K.; Boone, M.N.; Van Loo, D.; Dierick, M.; Van Acker, J.; Van den Bulcke, J. X-ray sub-micron tomography as a tool for the study of archaeological wood preserved through the corrosion of metal objects. *Archaeometry* **2012**, *54*, 893–905. [CrossRef]
36. Bird, M.I.; Ascough, P.L.; Young, I.M.; Wood, C.V.; Scott, A.C. X-ray microtomographic imaging of charcoal. *J. Archaeol. Sci.* **2008**, *35*, 2698–2706. [CrossRef]
37. Coubray, S.; Zech-Matterne, V.; Mazurier, A. The earliest remains of a Citrus fruit from a western Mediterranean archaeological context? A microtomographic-based re-assessment. *Comptes. Rendus. Palevol.* **2010**, *9*, 277–282. [CrossRef]
38. Mensa, F.S.; Muzzi, M.; Spani, F.; Tromba, G.; Dullin, C.; Di Giulio, A. When the Utility of Micro-Computed Tomography Collides with Insect Sample Preparation: An Entomologist User Guide to Solve Post-Processing Issues and Achieve Optimal 3D Models. *Appl. Sci.* **2022**, *12*, 769. [CrossRef]
39. Macchiarelli, R.; Bondioli, L.; Debénath, A.; Mazurier, A.; Tournepiche, J.F.; Birch, W.; Dean, M.C. How Neanderthal molar teeth grew. *Nature* **2006**, *444*, 748–751. [CrossRef] [PubMed]
40. Burrows, A.M.; Nash, L.T.; Hartstone-Rose, A.; Silcox, M.T.; López-Torres, S.; Selig, K.R. Dental signatures for exudativory in living primates, with comparisons to other gouging mammals. *Anat. Rec.* **2020**, *303*, 265–281. [CrossRef] [PubMed]
41. Andjelković, M.; Tomović, L.; Ivanović, A. Morphological integration of the kinetic skull in Natrix snakes. *J. Zool.* **2017**, *303*, 188–198. [CrossRef]
42. Spani, F.; Morigi, M.P.; Bettuzzi, M.; Scalici, M.; Carosi, M. A 3D journey on virtual surfaces and inner structure of ossa genitalia in Primates by means of a non-invasive imaging tool. *PLoS ONE* **2020**, *15*, e0228131.
43. Spani, F.; Morigi, M.P.; Bettuzzi, M.; Scalici, M.; Gentile, G.; Carosi, M. The ultimate database to (re) set the evolutionary history of primate genital bones. *Sci. Rep.* **2021**, *11*, 1–15.
44. Kendall, D.G. Shape manifolds, procrustean metrics, and complex projective spaces. *Bull. Lond. Math.* **1984**, *16*, 81–121. [CrossRef]
45. Bock, W.J. The definition and recognition of biological adaptation. *Am. Zool.* **1980**, *20*, 217–227. [CrossRef]
46. Gotthard, K.; Nylin, S. Adaptive plasticity and plasticity as an adaptation: A selective review of plasticity in animal morphology and life history. *Oikos* **1995**, *74*, 3–17. [CrossRef]
47. O'Higgins, P.; Cobb, S.N.; Fitton, L.C.; Gröning, F.; Phillips, R.; Liu, J.; Fagan, M.J. Combining geometric morphometrics and functional simulation: An emerging toolkit for virtual functional analyses. *J. Anat.* **2011**, *218*, 3–15. [CrossRef]
48. Dumont, M.; Wall, C.E.; Botton-Divet, L.; Goswami, A.; Peigné, S.; Fabre, A.-C. Do functional demands associated with locomotor habitat, diet, and activity pattern drive skull shape evolution in *Musteloid carnivorans*? *Biol. J. Lin. Soc.* **2016**, *117*, 858–878. [CrossRef]

49. Scalici, M.; Spani, F.; Traversetti, L.; Carpaneto, G.M.; Piras, P. Cranial shape parallelism in soft-furred sengis: Moving on a geographic gradient. *J. Mammal.* **2018**, *99*, 1375–1386. [CrossRef]
50. Spani, F.; Scalici, M.; Crandall, K.A.; Piras, P. Claw asymmetry in crabs: Approaching an old issue from a new point of view. *Biol. J. Linn. Soc.* **2020**, *129*, 162–176. [CrossRef]
51. Spani, F.; Scalici, M. Carapace asymmetries in crabs. *Crustaceana* **2018**, *91*, 1281–1290. [CrossRef]
52. Scalici, M.; Colamartino, M.; Spani, F.; Traversetti, L.; Persichini, T.; Maisano, M.; Fasulo, S.; Colasanti, M. Integrated early warning systems in marine bivalves reveal detrimental alterations of coastal habitats. *Hydrobiologia* **2020**, *847*, 2573–2585. [CrossRef]
53. Scalici, M.; Traversetti, L.; Spani, F.; Bravi, R.; Malafoglia, V.; Persichini, T.; Colasanti, M. Using 3D virtual surfaces to investigate molluscan shell shape. *Aquat. Living Resour.* **2016**, *29*, 207. [CrossRef]
54. Scalici, M.; Traversetti, L.; Spani, F.; Malafoglia, V.; Colamartino, M.; Persichini, T.; Cappello, S.; Mancini, G.; Guerriero, G.; Colasanti, M. Shell fluctuating asymmetry in the sea-dwelling benthic bivalve *Mytilus galloprovincialis* (Lamarck, 1819) as morphological markers to detect environmental chemical contamination. *Ecotoxicology* **2017**, *26*, 396–404. [CrossRef]
55. Ray, R.P.; Nakata, T.; Henningsson, P.; Bomphrey, R.J. Enhanced flight performance by genetic manipulation of wing shape in drosophila. *Nature Comm.* **2016**, *7*, 10851. [CrossRef]
56. Klein, L.L.; Caito, M.; Chapnick, C.; Kitchen, C.; O'Hanlon, R.; Chitwood, D.H.; Miller, A.J. Digital Morphometrics of two north American grapevines (*Vitis: Vitaceae*) quantifies leaf variation between species, within species, and among Individuals. *Front. Plant Sci.* **2017**, *8*, 373. [CrossRef]
57. Buchanan, B.; O'Brien, M.J.; Collard, M. Continent-wide or region-specific? A geometric morphometrics-based assessment of variation in Clovis point shape. *Archaeol. Anthropol. Sci.* **2014**, *6*, 145–162. [CrossRef]
58. Ros, J.; Evin, A.; Bouby, L.; Ruas, M.-P. Geometric morphometric analysis of grain shape and the identification of two-rowed barley (*Hordeum vulgare subsp. distichum* L.) in southern France. *J. Archaeol. Sci.* **2014**, *41*, 568–575. [CrossRef]
59. Ponton, D. Is geometric morphometrics efficient for comparing otolith shape of different fish species? *J. Morphol.* **2006**, *267*, 750–757. [CrossRef] [PubMed]
60. Weaver, A.A.; Schoell, S.L.; Stitzel, J.D. Morphometric analysis of variation in the ribs with age and sex. *J. Anat.* **2014**, *225*, 246–261. [CrossRef] [PubMed]
61. Frelat, M.A.; Katina, S.; Weber, G.W.; Bookstein, F.L. Technical note: A novel geometric morphometric approach to the study of long bone shape variation. *Am. J. Phys. Anthrop.* **2012**, *149*, 628–638. [CrossRef] [PubMed]
62. Gardiner, J.D.; Behnsen, J.; Brassey, C.A. Alpha shapes: Determining 3D shape complexity across morphologically diverse structures. *BMC Evol. Biol.* **2018**, *18*, 184. [CrossRef] [PubMed]
63. Brassey, C.A.; Behnsen, J.; Gardiner, J.D. Postcopulatory sexual selection and the evolution of shape complexity in the carnivoran baculum. *Proc. Royal Soc. B* **2020**, *287*, 20201883. [CrossRef] [PubMed]
64. Arnqvist, G.; Thornhill, R.; Rowe, L. Evolution of animal genitalia: Morphological correlates of fitness components in a water strider. *J. Evol. Biol.* **1997**, *10*, 613–640. [CrossRef]
65. Holwell, G.I.; Winnick, C.; Tregenza, T.; Herberstein, M.E. Genital shape correlates with sperm transfer success in the praying mantis *Ciulfina klassi* (*Insecta: Mantodea*). *Behav. Ecol. Sociobiol.* **2010**, *64*, 617–625. [CrossRef]
66. Macagno, A.L.M.; Pizzo, A.; Parzer, H.F.; Palestrini, C.; Rolando, A.; Moczek, A.P. Shape—but not size—Codivergence between male and female copulatory structures in Onthophagus beetles. *PLoS ONE* **2011**, *6*, e28893. [CrossRef]
67. Simmons, L.W.; Firman, R.C. Experimental evidence for the evolution of the mammalian baculum by sexual selection. *Evolution* **2013**, *68*, 276–283. [CrossRef]
68. Hopwood, P.E.; Head, M.L.; Jordan, E.J.; Carter, M.J.; Davey, E.; Moore, A.J.; Royle, N.J. Selection on an antagonistic behavioral trait can drive rapid genital coevolution in the burying beetle, *Nicrophorus vespilloides*. *Evolution* **2016**, *70*, 1180–1188. [CrossRef]
69. Pizzo, A.; Mercurio, D.; Palestrini, C.; Roggero, A.; Rolando, A. Male differentiation patterns in two polyphenic sister species of the genus *Onthophagus Latreille*, 1802 (*Coleoptera: Scarabaeidae*): A geometric morphometric approach. *J. Zool. Syst. Evol. Res.* **2006**, *44*, 54–62. [CrossRef]
70. Dinca, V.; Dapporto, L.; Vila, R. A combined genetic-morphometric analysis unravels the complex biogeographical history of *Polyommatus icarus* and *Polyommatus celina* common blue butterflies. *Mol. Ecol.* **2011**, *20*, 3921–3935. [CrossRef] [PubMed]
71. Edelsbrunner, H.; Mücke, E.P. Three-dimensional alpha shapes. *ACM Trans. Graph.* **1994**, *13*, 43–72. [CrossRef]
72. Rohlf, F.J.; Slice, D. Extensions of the Procrustes method for the optimal superimposition of landmarks. *Sys. Biol.* **1990**, *39*, 40–59. [CrossRef]
73. Hill, O.W.C. I-Strepsirrhini. In *Primates-Comparative Anatomy and Taxonomy*; University Press: Edinburgh, UK, 1953; p. 798.
74. Harms, J.W. *Primatologia—Handbook of Primatology*; Hofer, H., Schultz, A.H., Starck, D., Eds.; Karger: Basel, Switzerland, 1956; Volume I, p. 1063.
75. von Pehrson, T. Beiträge zur Kenntnis der äusseren weiblichen Genitalien bei Affen, Halbaffen, und Insectivoren. *Anat. Anz.* **1914**, *46*, 161–179.
76. von Pohl, L. Beitrage zur Kenntnis des Os penis der Prosimier. *Anat. Anz.* **1910**, *37*, 225–231.
77. Brindle, M.; Opie, C. Postcopulatory sexual selection influences baculum evolution in primates and carnivores. *Proc. Royal Soc. B* **2016**, *283*, 20161736. [CrossRef]
78. Dixson, A.F. Observations on the evolution of the genitalia and copulatory behaviour in male primates. *J. Zool.* **1987**, *213*, 423–443. [CrossRef]

79. Dixson, A.; Nyholt, J.; Anderson, M. A positive relationship between baculum length and prolonged intromission patterns in mammals. *Acta Zool. Sin.* **2004**, *50*, 490–503.
80. Verrell, P.A. Primate penile morphologies and social systems: Further evidence for an association. *Folia Primatol.* **1992**, *59*, 114–120. [CrossRef]
81. Ramm, S.A. Sexual selection and genital evolution in mammals: A phylogenetic analysis of baculum length. *Am. Nat.* **2007**, *169*, 360–369. [CrossRef] [PubMed]
82. Pomidor, B.J.; Makedonska, J.; Slice, D.E. A Landmark-Free Method for Three-Dimensional Shape Analysis. *PLoS ONE* **2016**, *11*, e0150368. [CrossRef] [PubMed]
83. Besl, P.J.; McKay, N.D. Method for registration of 3-D shapes. *Proc. SPIE* **1992**, *1611*, 586–607. [CrossRef]
84. Chen, Y.; Medioni, G. Object modelling by registration of multiple range images. *Image Vis. Comput.* **1992**, *10*, 145–155. [CrossRef]
85. Dixson, A.F. Baculum length and copulatory behavior in primates. *Am. J. Primatol.* **1987**, *13*, 51–60. [CrossRef]
86. Dixson, A.F. *Primate Sexuality: Comparative Studies of the Prosimians, Monkeys, Apes, and Humans, 2nd ed*; Oxford University Press: Oxford, UK, 2012; p. 808.
87. Romer, S.A. *The Vertebrate Body*; Saunders: Philadelphia, PA, USA, 1962; p. 627.
88. Hill, O.W.C. *Evolutionary Biology of Primates*; Academic Press: London, UK, 1972; p. 233.
89. Hershkovitz, P. 14. External genitalia and accessory structures. In *Living New World Monkeys (Platyrrhini) with an Introduction to Primates*; Hershkovitz, P., Ed.; The University Chicago Press: Chicago, IL, USA, 1977; Volume 1, pp. 112–119.
90. Hershkovitz, P. Male external genitalia of non-prehensile tailed South-American monkeys. Part, I. Subfamily Pitheciinae, Family Cebidae. *Fieldiana Zool.* **1993**, *73*, 1–17.
91. Stockley, P. The baculum. *Curr. Biol.* **2012**, *22*, R1032–R1033. [CrossRef]
92. Lough-Stevens, M.; Schultz, N.G.; Dean, M.D. The baubellum is more developmentally and evolutionarily labile than the baculum. *Ecol. Evol.* **2018**, *8*, 1073–1083. [CrossRef]
93. Ah-King, M.; Barron, A.B.; Herberstein, M.E. Genital evolution: Why are females still understudied? *PLoS Biol.* **2014**, *12*, e1001851. [CrossRef]
94. Estrada, A.; Garber, P.A.; Rylands, A.B.; Roos, C.; Fernandez-Duque, E.; Di Fiore, A.; Nekaris, K.A.I.; Nijman, V.; Heymann, E.W.; Lambert, J.E.; et al. Impending extinction crisis of the world's primates: Why primates matter. *Sci. Adv.* **2017**, *3*, e1600946. [CrossRef]
95. Carosi, M.; Spani, F.; Ulland, A.E.; Scalici, M.; Suomi, S.J. Clitoral length in immature and mature captive tufted capuchin (*Sapajus spp.*) females: A cross-sectional study. *Am. J. Primatol.* **2020**, *82*, e23135. [CrossRef] [PubMed]